Euro. Jnl of Applied Mathematics (2012), *vol.* 23, *pp.* 181–200.
doi:10.1017/S0956792510000343

A perturbative approach to the backflow dynamics of nematic defects

PAOLO BISCARI[1] and TIMOTHY J. SLUCKIN[2]

[1]*Dipartimento di Matematica, Politecnico di Milano, Piazza Leonardo da Vinci 32, 20133 Milan, Italy*
email: paolo.biscari@polimi.it

[2]*School of Mathematics, University of Southampton, Southampton SO17 1BJ, UK*
email: t.j.sluckin@soton.ac.uk

(*Received 18 November 2010; revised 23 November 2010; accepted 30 November 2010; first published online 5 January 2011*)

We present an asymptotic theory that includes in a perturbative expansion the coupling effects between the director dynamics and the velocity field in a nematic liquid crystal. Backflow effects are most significant in the presence of defect motion, since in this case the presence of a velocity field may strongly reduce the total energy dissipation and thus increase the defect velocity. As an example, we illustrate how backflow influences the speeds of opposite-charged defects.

Key words: Nematic liquid crystals; Perturbations, asymptotics; propagation of defects

1 Introduction

Liquid crystals were first wrongly recognised as such from the dramatic patterns, which appeared when they were observed in a microscope between crossed polarizers. In the case of nematic liquid crystals, the defining feature of these patterns was a set of points and associated dark lines that were invariant with respect to rotation of the polarizers. The pattern has now come to be known as the Schlieren texture, after the German word for stain. Some time later, it was the lines which prompted Friedel [1] to name the phase *nematic*, after the Greek word for thread.

The length scale of the Schlieren texture is, of course, not fine enough to observe the microscopic structure of the anisotropic nematic phase. But texture does probe topological singularities in the order parameter field, or more specifically, the mapping between real space $\mathbf{R}^3$ and the equilibrium nematic order parameter manifold $\mathbf{RP}^2$. By using homotopy groups, the topological theory of defects in condensed matter systems develops relations between the topology of the equilibrium order parameter manifold and the allowed order parameter defect structures [2–5]. The task of connecting liquid crystal textures with the underlying molecular structures originally required Herculean intellectual strength. But modern mathematics has reduced this to a straightforward computational procedure.

Although the evidence of the defects in the director field dominates our macroscopic view of nematic liquid crystals, initial theoretical progress in treating both the statics and dynamics neglected the defect structure. Both Oseen [6] and Frank [7] in their pioneering works display elaborate diagrams of what Frank called *disinclinations* (later renamed as *disclinations* by a somewhat mysterious historical process). But their seminal

works develop free energies of weakly inhomogeneous nematics, from which all hints of singularities in the director field have been been excised. Likewise, Ericksen [8–10], and later Leslie [11], in their development of a consistent nematodynamics, suppose that the director is everywhere well defined, and develop stress tensor descriptions in terms of rates of change and inhomogeneities in the director and velocity fields.

It was only later, after the theoretical structure of disclination-free nematics had been well understood, that defect problems once again became a primary focus of research. Key questions are, firstly, what is the molecular organisation in the core of a disclination line, and secondly, how does a disclination line (or assembly of lines) move in a nematic fluid. A subsidiary question, still open at the time of writing, concerns the extent to which details of the internal structure are important in determining defect motion.

There are two basic strategies that have been adopted in order to understand defect motion and structure. On the one hand one can follow what elsewhere in material science is known as the *phase field* strategy. A phase field in the context of crystallization dynamics involves the introduction of an artificial order parameter describing the degree of crystallization. In so doing, one turns a difficult free boundary problem into a (relatively!) easy differential problem. In the context of nematic liquid crystals, the idea is to embed the Oseen–Frank–Leslie–Ericksen director picture minimally into a more general-order parameter picture. The relevant free energy was first written down by de Gennes [12] in terms of what was then known as the Saupe ordering matrix, but which is now known as the **Q**-tensor [13–15]. However, it is important to note that here the **Q**-tensor is a phase field with a real molecular meaning, unlike some phase fields used elsewhere. Under suitable conditions, the **Q**-tensor defines a single vector $\mathbf{n} \equiv -\mathbf{n}$, and then the macroscopic theories are valid. But in the core of the defect, it is no longer possible to define the director **n**. This was the strategy adopted by Schopohl and one of the authors long ago [16] when discussing the disclination core structure.

An alternative route to dealing with defect cores in a domain where the director can otherwise be regularly defined is simply to excise it. The region surrounding the core is then treated as a (possibly moving!) surface of the dynamic problem. This kind of method goes back to Volterra's pioneering attempts to understand stresses and strains in non-simply connected domains [17]. This work motivated Volterra to introduce what he called *distorsioni* (later relabelled in English by Love as *dislocations* [18]). These ideas were later taken up, rather imaginatively, by Burgers [19] when he treated microscopic irregularities in crystal structures. The moving surfaces surrounding the disclinations are now incorporated in a dynamical structure using the usual kind of force balance arguments. The practical downside of this type of procedure is that now it is required to solve a difficult free boundary problem. A more theoretical drawback involves defining precise criteria for the location of the excising surface, and knowing that there is a precise analytical process, which ensures the existence of correct and sensible limits in cases when, for example, the defects are moving at some speed.

At this stage, there is no consensus in the liquid crystal community as to which of these procedures is more fruitful or easier. Indeed, it is not even clear whether they are different routes to the same truth, or rather represent non-trivially different approaches. In this paper, we use the *cut-off* strategy to gain some insight into the motion of disclination lines, and the consequent motion of the nematic itself, in a two-dimensional nematic, which

https://doi.org/10.1017/S0956792510000343 Published online by Cambridge University Press

means that the nematic director lies in a plane, and that the space is regarded as being homogeneous in a direction parallel to the direction of the defect lines. We compare our results with the results of simulations adopting the **Q**-tensor approach. The fact that there is some qualitative resemblance between the results of calculations using rather different philosophies may be regarded as circumstantial evidence that the *many-roads-to-the-truth* picture is correct.

The analogy between topological defects in broken-symmetry condensed matter systems and charges in electromagnetism has been very seductive. In electromagnetism, charges are conserved, apparently by divine intervention, and can either be considered to interact at a distance or to interact with fields whose sources are other charges, subject to specific boundary conditions. The charges then move in the force fields of other charges.

In broken-symmetry condensed matter systems too, topological charges are (more-or-less!) rigidly conserved. But now, of course, the basis for the conservation law can be readily understood in terms of the topological properties of the underlying order parameter field. There is a strong temptation to try to construct theories in which the topological charges (in our case, the strength of nematic disclination lines) also interact at a distance, or through fields whose sources are the other defect lines. In this picture the actual director structure, the core of the normal continuum nematic theory, could somehow be integrated out of the problem. In this way, for example, one could calculate the force field on a disclination line, presumably by looking at the inhomogeneous director structure in the absence of the disclination line in question. The motion would then be determined, omitting inertial effects, by calculating the drag force on a moving defect line, and balancing it with the external force. This kind of approach has been adopted by Ryskin and Kremenetsky [20–22].

A particular complication of the moving nematic defect problem is that the defect line is a structure, rather than an object. In the simplest toy models of nematodynamics, there is no interaction between the orientational degrees of freedom and dynamics degrees of freedom. Orientational relaxation takes place through the time-dependent Ginzburg–Landau (TDGL) equation (equivalently, a balance between orientational dissipation and energy loss), and there is no necessary fluid motion associated with the relaxation. But even in this approach, defect motion (and mutual defect annihilation) can occur. But, in fact, the TDGL approach is inadequate for describing director relaxation. A system out of orientational equilibrium sustains an unbalanced stress tensor, causing fluid motion as well as rotation, a phenomenon which has come to be known as *backflow* [23].

The general problem of moving defects attracts the interest of fundamental theorists who want to build theories in which orientational degrees of freedom are coupled to charge-like positionally restricted defects. Some analogies have been drawn with defects in gauge theories of elementary particles with applications, for example, to cosmic strings in the early universe [24]. But a more mundane motivation in the context of liquid crystals concerns the ubiquity of disclination lines in nematic textures, and the importance of understanding the motion of these lines, for example in switching in bistable devices [25].

In this paper we take the latter approach, which requires us to study some specific well-defined problems. These problems are as follows: (a) The motion of a single disclination line, and the consequent fluid motion (backflow), in the presence of an electric or magnetic

field (problem A), and (b) the mutual motion of a pair of disclination lines (problem B). The latter sometimes involves initial attraction, and subsequent mutual annihilation. In this discussion we shall confine our interest to line defects, which are ubiquitous in nematic liquid crystals, and two-dimensional objects. The analogous three-dimensional objects – point defects or the so-called hedgehogs, with somewhat analogous properties [24, 26–29] – are rarer, perhaps for profound topological reasons [30].

There has been previous work on problems A and B. Richardson [31] studied a model disclination in which the disclination motion induces fluid motion, but not *vice versa*. In a previous paper [32] we have discussed both problems A and B, using a cut-off approach. In the case when splay and bend elasticities were equal, both the unzipping of a disclination line in a field (problem A) and the time to mutual annihilation (problem B) were independent of the topological sign of defects. But extensive numerical studies of **Q**-tensor model dynamics, using both the Lattice Boltzmann approach [33–35], and a more conventional hydrodynamic algorithm [36] give rise to a similar picture. But a key question in disclination dynamics concerns the qualitative effect of backflow on the disclination motion. Both groups find that backflow influences the annihilation time of mutually attracting defects (problem B), causing it to depend on the topological signature of the defects. In addition, Svenšek and Žumer [36] also find (problem A) that the unzipping speed depends on topological signature, a general picture which has also been confirmed experimentally [37].

However, these studies are numerical. In the general case, it seems that detailed prediction in these complex systems requires a good deal of computation [38–44]. Sonnet and Virga [45], by contrast, have written down general equations of motion for dislocation motion, although at the time of writing, this approach has not yet been used to study any practical cases. But the precise manner in which backflow affects the disclination motion should be susceptible to more than just a computational approach.

This paper addresses specifically problem A, building on our previous paper [32], within an approach which includes backflow, and a special limiting case, the no-backflow case considered in [32]. Nevertheless, it turns out that some of the outcomes provide an explanation for the difference in speeds observed when studying problem B. In order to carry through this program, we build a theory in which the backflow interactions are turned on perturbatively in a controlled fashion. In our approach the perturbation parameter is essentially a dimensionless inverse density, the ratio between the Leslie and Newtonian viscosities. Thus, in the limit $\epsilon \to 0$, orientational relaxation fails to excite any fluid motions. By contrast with the computational studies discussed above, our calculations do not seek an accurate numerical solution for problems A and B. Rather we aim to illuminate the specific role of backflow in distinguishing between the motion of disclinations of opposite topological signature. Also by contrast with these approaches we do not use the **Q**-tensor theory, but rather the cut-off Ericksen–Leslie approach, in which the core of the defect line plays an insignificant role. Qualitative agreement with the more precise numerical solutions validates our approach *ex post facto*.

Despite the simplifications introduced by the perturbative expansion we perform, the Ericksen–Leslie equations remain far too complex to allow for an analytical solution. As an alternative strategy, we turn to a theorem by Leonov [46], which proves that the actual velocity field minimises the dissipation functional $\mathscr{D}$ at fixed director field. The variational principle represents a quite powerful tool, because it allows us to approximate the exact

solution of the Ericksen–Leslie equations by finding the best guess in suitable classes of velocity fields.

The plan of the paper is as follows. In the next section we briefly review the general equations of motion of nematic liquid crystals. In Sections 3 and 4 we set up the perturbative expansion and the variational principle that allow to gain insight into the backflow field induced by the motion of a stationary pattern. In Section 5 we apply the methods developed above to the planar motion of a nematic disclination. A concluding section reviews the main results and sets up the bases for future related work.

2 Nematic liquid crystals: dynamic equations

In this section we briefly review the Ericksen–Leslie theory for the dynamics of nematic liquid crystals. This summary is intended to introduce the equations of motion that will be discussed in the following. Let $\mathbf{n}$ and $\mathbf{u}$ denote the director and the velocity fields. Then $\mathbf{n}$ is, as usual, a unit vector field, possibly singular at the defect points, while $\mathbf{u}$ will be assumed to be continuous everywhere, and differentiable almost everywhere.

The Ericksen–Leslie dynamic equations will be introduced following the classical notation. For their derivation the reader may refer, e.g. to the classical book by de Gennes and Prost [47]. The balance of linear momentum dictates

$$\rho\,\dot{\mathbf{u}} = \operatorname{div}\mathbf{T}, \tag{2.1}$$

where ρ is the fluid density. The stress tensor $\mathbf{T}$ can be decomposed as $\mathbf{T} = \mathbf{T}^{(\mathrm{E})} + \mathbf{T}^{(\mathrm{i})}$, where the Ericksen stress $\mathbf{T}^{(\mathrm{E})}$ and the irreversible stress $\mathbf{T}^{(\mathrm{i})}$ are defined as

$$\begin{aligned}\mathbf{T}^{(\mathrm{E})} &:= -p\,\mathbf{I} + \sigma\,\mathbf{I} - (\boldsymbol{\nabla}\mathbf{n})^T\,\frac{\partial\sigma}{\partial\boldsymbol{\nabla}\mathbf{n}} \quad \text{and}\\ \mathbf{T}^{(\mathrm{i})} &:= \alpha_1\,(\mathbf{n}\cdot\mathbf{D}\mathbf{n})\,\mathbf{n}\otimes\mathbf{n} + \alpha_2\,\mathbf{N}\otimes\mathbf{n} + \alpha_3\,\mathbf{n}\otimes\mathbf{N} + \alpha_4\,\mathbf{D}\\ &\quad + \alpha_5\,\mathbf{D}\mathbf{n}\otimes\mathbf{n} + \alpha_6\,\mathbf{n}\otimes\mathbf{D}\mathbf{n}.\end{aligned} \tag{2.2}$$

In the above decomposition, $\sigma = \sigma_{\mathrm{F}} + \sigma_H$ is the free energy density, which includes the Frank elastic energy density σ_{F} and the external field energy density σ_H. Furthermore, p is the hydrodynamic pressure, $\mathbf{I}$ is the identity tensor, $\mathbf{D}$ is the rate of strain tensor and $\{\alpha_1,\ldots,\alpha_6\}$ are the Leslie viscosities. Finally, $\mathbf{N} := \dot{\mathbf{n}} - \boldsymbol{\omega}\wedge\mathbf{n}$ is the rate of change of the director with respect to the background fluid, since $\boldsymbol{\omega} = \frac{1}{2}\operatorname{curl}\mathbf{u}$.

On the other hand, the balance of angular momentum sets

$$\gamma_1\,\mathbf{N} + \gamma_2\,\mathbf{D}\mathbf{n} = \operatorname{div}\frac{\partial\sigma}{\partial\boldsymbol{\nabla}\mathbf{n}} - \frac{\partial\sigma}{\partial\mathbf{n}} + \mu\,\mathbf{n} =: \mathbf{h}, \tag{2.3}$$

where γ_1 and γ_2 are defined in term of Leslie's coefficients as

$$\gamma_1 := \alpha_3 - \alpha_2, \qquad \gamma_2 := \alpha_2 + \alpha_3 = \alpha_6 - \alpha_5, \tag{2.4}$$

$\mathbf{h}$ is the molecular field and μ is the Lagrange multiplier that keeps $|\mathbf{n}|$ fixed. We remark that the second equation in (2.4) assumes the validity of the Onsager–Parodi relation [48]. If we make use of (2.3), the divergence of the Ericksen stress tensor can be given the

https://doi.org/10.1017/S0956792510000343 Published online by Cambridge University Press

following form:

$$\operatorname{div} \mathbf{T}^{(\mathrm{E})} = -\boldsymbol{\nabla} p + (\boldsymbol{\nabla}\mathbf{n})^T \left(\frac{\partial \sigma}{\partial \mathbf{n}} - \operatorname{div} \frac{\partial \sigma}{\partial \boldsymbol{\nabla}\mathbf{n}} \right) = -\boldsymbol{\nabla} p - (\boldsymbol{\nabla}\mathbf{n})^T (\gamma_1 \mathbf{N} + \gamma_2 \mathbf{D}\mathbf{n}),$$

where the μ-term has been dropped because $(\boldsymbol{\nabla}\mathbf{n})^T \mathbf{n} = \mathbf{0}$.

Equations (2.1) and (2.3), together with the incompressibility condition

$$\operatorname{div} \mathbf{u} = 0 \tag{2.5}$$

and the boundary/initial conditions allow us in principle to determine the unknown fields $\mathbf{n}$, $\mathbf{u}$ and p.

In the present paper we will analyse a planar problem. We will thus assume that both $\mathbf{n}$ and $\mathbf{u}$ are everywhere orthogonal to a fixed direction $\mathbf{e}_z$, and that all dynamic fields depend only on the planar coordinates (x, y). Consistently, we identify the director through a tilt angle ϕ, defined such as $\mathbf{n} = \cos\phi\, \mathbf{e}_x + \sin\phi\, \mathbf{e}_y$.

We look for stationarily travelling solutions, and assume that there exists $\mathbf{v}$ (to be determined) such that

$$f(\mathbf{x}, t) = f(\mathbf{x} - \mathbf{v}t, 0) \qquad \text{for all } \mathbf{x} \text{ and } t, \tag{2.6}$$

where $\mathbf{v}$ is the pattern velocity and f may be any component of $\mathbf{n}$ or $\mathbf{u}$, or the pressure field p. In particular

$$\dot{f} = -\mathbf{v} \cdot \boldsymbol{\nabla} f \qquad \text{and} \qquad (\boldsymbol{\nabla} f)^{\bullet} = -(\boldsymbol{\nabla}^2 f)\mathbf{v}.$$

We adopt the one-constant approximation for the Frank elastic energy density, so that

$$\sigma_{\mathrm{F}}(\mathbf{n}, \boldsymbol{\nabla}\mathbf{n}) = \tfrac{1}{2} K\, |\boldsymbol{\nabla}\mathbf{n}|^2,$$

and consider a constant external magnetic field such that

$$\sigma_H(\mathbf{n}) = -\tfrac{1}{2}\, \chi_{\mathrm{a}}\, (\mathbf{n} \cdot \mathbf{H})^2,$$

where $\chi_{\mathrm{a}} > 0$ is the diamagnetic anisotropy. We fix the x-direction to be parallel to the external field $\mathbf{H}$ and, by making reference to the similar geometry as analysed in [32], we expect the velocity of the stationary pattern to be parallel to the external field: $\mathbf{v} = v\, \mathbf{e}_x$. When this is the case, we have

$$\begin{aligned} \boldsymbol{\nabla}\mathbf{n} &= \mathbf{n}_\perp \otimes \boldsymbol{\nabla}\phi, \quad \text{where} \quad \mathbf{n}_\perp := -\sin\phi\, \mathbf{e}_x + \cos\phi\, \mathbf{e}_y, \\ (\boldsymbol{\nabla}\mathbf{n})^T \frac{\partial \sigma_{\mathrm{F}}}{\partial \boldsymbol{\nabla}\mathbf{n}} &= K (\boldsymbol{\nabla}\mathbf{n})^T \boldsymbol{\nabla}\mathbf{n} = K\, \boldsymbol{\nabla}\phi \otimes \boldsymbol{\nabla}\phi, \quad \text{and} \\ \mathbf{T}^{(\mathrm{E})} &= \left(\frac{K}{2} |\boldsymbol{\nabla}\phi|^2 - \frac{1}{2}\, \chi_{\mathrm{a}}\, (\mathbf{n} \cdot \mathbf{H})^2 - p \right) \mathbf{I} - K\, \boldsymbol{\nabla}\phi \otimes \boldsymbol{\nabla}\phi. \end{aligned}$$

https://doi.org/10.1017/S0956792510000343 Published online by Cambridge University Press

3 A perturbative backflow expansion

The dynamic equations (2.1), (2.3) and (2.5) have been thoroughly studied in the *no-backflow* approximation. Such an approximation amounts to neglecting the coupling terms between the nematic director and the velocity fields. Much less is known in the general case, since solving the complete system is a formidable task, and can be typically attacked only through numerical simulations and/or in very simple geometries [23]. The main purpose of the present section is to derive an expansion that permits the inclusion of backflow effects in a perturbative way. Such an expansion highlights the coupling terms that first influence the nematic field. It also permits the derivation of a simplified set of dynamic equations, which, at least in the stationary case, eventually provides analytical insight into the structure of the velocity field induced by the director orientation.

The no-backflow approximation amounts to neglecting all the Leslie coefficients, which couple $\mathbf{n}$ and $\mathbf{u}$: α_1, α_2, α_3, α_5, α_6. We remark that the macroscopic viscosity α_4 is not included in this list, since it represents the Newtonian viscosity and is not related to the anisotropic character of nematic liquid crystals.

From the mathematical point of view, the no-backflow approximation can be derived as the zero-th order solution of the following perturbative problem. We introduce a small, dimensionless parameter ϵ in order to emphasize that α_4 (and, consequently, the density ρ) are much greater than the remaining α_is:

$$\rho = \frac{\tilde{\rho}}{\epsilon} \qquad \alpha_4 = \rho\nu = \frac{\tilde{\alpha}_4}{\epsilon}, \tag{3.1}$$

where ν is the kinematic viscosity. The scaled density and the Newtonian viscosity $\tilde{\rho}$ and $\tilde{\alpha}_4$ are then assumed to be of the same order for the remaining α_is. Before we explicitly start using (3.1), it is worthwhile to remark that a formal definition of the small parameter ϵ can be obtained by setting $\epsilon := \max\{|\alpha_1|, |\alpha_2|, |\alpha_3|, |\alpha_5|, |\alpha_6|\}/\alpha_4$, and then defining $\tilde{\alpha}_4 = \epsilon\alpha_4$, and $\tilde{\rho} = \epsilon\rho$. We remark that in practical situations it is definitely not always true that the Newtonian viscosity α_4 is much larger than all the remaining nematic viscosities (see, e.g. [49], p. 330). When this is the case, backflow effects must be expected to be consistent. Consequently, the perturbative expansion that we are introducing will only be able to catch the first correction to be introduced, though not the precise features of the solution. There is, however, a case in which our approximation is always valid. When the temperature approaches to nematic–isotropic transition, the nematic viscosities are strongly reduced and become all much smaller than the Newtonian viscosity.

In order to implement the perturbative expansion, we expand all relevant fields as

$$\mathbf{u} = \epsilon\,\mathbf{u}_1 + o(\epsilon), \quad \mathbf{n} = \mathbf{n}_0 + \epsilon\,\mathbf{n}_1 + o(\epsilon), \quad p = p_0 + \epsilon\,p_1 + o(\epsilon), \quad \text{as } \epsilon \to 0. \tag{3.2}$$

The $O(1)$ terms from equation (2.5), and the $O(\epsilon^{-1})$ terms from equation (2.1) (which arise by virtue of (3.1)) are identically satisfied because $\mathbf{u}_0 \equiv \mathbf{0}$. In order to analyse equation (2.3) we notice that

$$\mathbf{N} = \dot{\mathbf{n}} + O(\epsilon) = -(\boldsymbol{\nabla}\mathbf{n}_0)\mathbf{v}_0 + O(\epsilon) =: \mathbf{N}_0 + O(\epsilon),$$

https://doi.org/10.1017/S0956792510000343 Published online by Cambridge University Press

where $\mathbf{v}_0 = v_0\,\mathbf{e}_x$ is the leading contribution to the pattern velocity. If we project out the μ-term by performing a vector multiplication by $\mathbf{n}_0$, then we obtain

$$K\,\Delta\phi_0 + \gamma_1\,v_0\phi_{0,x} + \chi_a\,H^2\sin\phi_0\cos\phi_0 = 0. \tag{3.3}$$

Equation (3.3) has been analytically studied, e.g. in [32] to obtain the no-backflow approximation to the speed of a disclination moving in an external magnetic field. It was shown that the speed v_0 can be found by solving a suitable eigenvalue problem, which, in physical terms, ensures that the motion is sustained without any energy flux from the infinity.

The leading order of the velocity field follows from the $O(1)$-terms of equation (2.1) and the $O(\epsilon)$-term of equation (2.5), which yield

$$\begin{aligned}\tilde{\rho}\,\dot{\mathbf{u}}_1 = -\tilde{\rho}\,v_0\,\mathbf{u}_{1,x} &= -\boldsymbol{\nabla}p_0 - (\alpha_3-\alpha_2)\,(\boldsymbol{\nabla}\mathbf{n}_0)^T\mathbf{N}_0 \\ &\quad + \operatorname{div}(\alpha_2\,\mathbf{N}_0\otimes\mathbf{n}_0 + \alpha_3\,\mathbf{n}_0\otimes\mathbf{N}_0 + \tilde{\alpha_4}\operatorname{sym}\boldsymbol{\nabla}\mathbf{u}_1), \qquad (3.4)\\ \operatorname{div}\mathbf{u}_1 &= 0. \qquad (3.5)\end{aligned}$$

By using (3.5), equation (3.4) can be rewritten as

$$\begin{aligned}\tfrac{1}{2}\tilde{\alpha_4}\Delta\mathbf{u}_1 + \tilde{\rho}\,v_0\,\mathbf{u}_{1,x} &= \boldsymbol{\nabla}p_0 + 2\alpha_2\,(\boldsymbol{\nabla}\phi_0\cdot\mathbf{v}_0)\,\boldsymbol{\nabla}\phi_0 + \alpha_2((\boldsymbol{\nabla}^2\phi_0)\mathbf{v}_0\cdot\mathbf{n}_0)\mathbf{n}_{\perp 0} \\ &\quad - 2\gamma_2\,(\boldsymbol{\nabla}\phi_0\cdot\mathbf{v}_0)\,(\boldsymbol{\nabla}\phi_0\cdot\mathbf{n}_0)\mathbf{n}_0 + \alpha_3((\boldsymbol{\nabla}^2\phi_0)\mathbf{v}_0\cdot\mathbf{n}_{\perp 0})\mathbf{n}_0. \qquad (3.6)\end{aligned}$$

In order to get rid of the pressure term, we can take the curl of equation (3.6) and obtain an equation of the form

$$\Delta(\operatorname{curl}\mathbf{u}_1) + \frac{2\tilde{\rho}\,v_0}{\tilde{\alpha}_4}\operatorname{curl}\mathbf{u}_{1,x} = \mathbf{U}(x,y),$$

where the source term $\mathbf{U}$ can be written in terms of the zero-th order expressions for the director and the pattern velocity. As a result, we obtain a linear elliptic PDE for $\operatorname{curl}\mathbf{u}_1$ that, in principle, can be solved by using the same Fourier-transform methods described in [32]. Were we able to solve it explicitly, we would end up with the system

$$\operatorname{curl}\mathbf{u}_1(x,y) = \Omega(x,y)\,\mathbf{e}_z, \qquad \operatorname{div}\mathbf{u}_1(x,y) = 0. \tag{3.7}$$

In turn, equation (3.7) can be analytically solved by using the vorticity-stream formulation for 2D flows (see, e.g. [50], §2.1). One obtains

$$\mathbf{u}_1(\mathbf{x}) = \mathbf{u}_{1\infty} + \frac{1}{2\pi}\int_{\mathbb{R}^2}\frac{\Omega(\mathbf{x}')}{|\mathbf{x}-\mathbf{x}'|^2}\,\mathbf{e}_z\wedge(\mathbf{x}-\mathbf{x}')\,\mathbf{d}\mathbf{x}'.$$

Though, in principle, all the above steps are affordable, a glance to equation (3.6) suffices to convince ourselves that the result is still far from being easy to interpret. That is why in Section 4 we will combine the perturbative expansion just introduced with a suitable variational argument to identify an optimisation problem, which will eventually provide the physical information we aim at extracting from the dynamic equations.

https://doi.org/10.1017/S0956792510000343 Published online by Cambridge University Press

3.0.1 *Perturbation of the director*

Let us now analyse the $O(\epsilon)$ term in equation (2.3). At first order

$$\begin{aligned}\mathbf{N} &= \dot{\mathbf{n}} - \boldsymbol{\omega} \wedge \mathbf{n} = -(\boldsymbol{\nabla}\mathbf{n})\mathbf{v} - \boldsymbol{\omega} \wedge \mathbf{n} \\ &= -(\boldsymbol{\nabla}\mathbf{n}_0)\mathbf{v}_0 - \epsilon(\boldsymbol{\nabla}\mathbf{n}_1)\mathbf{v}_0 - \epsilon(\boldsymbol{\nabla}\mathbf{n}_0)\mathbf{v}_1 - \epsilon\,\boldsymbol{\omega}_1 \wedge \mathbf{n}_0 + o(\epsilon).\end{aligned}$$

Moreover,

$$\operatorname{div}\frac{\partial\sigma}{\partial\boldsymbol{\nabla}\mathbf{n}} - \frac{\partial\sigma}{\partial\mathbf{n}} = K\Delta\mathbf{n}_0 + \chi_a(\mathbf{n}_0\cdot\mathbf{H})\mathbf{H} + \epsilon K\Delta\mathbf{n}_1 + \epsilon\chi_a(\mathbf{n}_1\cdot\mathbf{H})\mathbf{H} + o(\epsilon),$$

so that the $O(\epsilon)$ contribution to equation (2.3) requires

$$\begin{aligned}&-\gamma_1\mathbf{n}_0\wedge(\boldsymbol{\nabla}\mathbf{n}_1)\mathbf{v}_0 - \gamma_1\mathbf{n}_0\wedge(\boldsymbol{\nabla}\mathbf{n}_0)\mathbf{v}_1 - \gamma_1\mathbf{n}_0\wedge(\boldsymbol{\omega}_1\wedge\mathbf{n}_0) - \gamma_1\mathbf{n}_1\wedge(\boldsymbol{\nabla}\mathbf{n}_0)\mathbf{v}_0 \\ &+\gamma_2\,\mathbf{n}_0\wedge\mathbf{D}\mathbf{n}_0 = K\,\mathbf{n}_1\wedge\Delta\mathbf{n}_0 + \chi_a(\mathbf{n}_0\cdot\mathbf{H})\mathbf{n}_1\wedge\mathbf{H} + K\,\mathbf{n}_0\wedge\Delta\mathbf{n}_1 + \chi_a(\mathbf{n}_1\cdot\mathbf{H})\mathbf{n}_0\wedge\mathbf{H},\end{aligned}$$

where the pattern velocity has been expanded as well: $\mathbf{v} = \mathbf{v}_0 + \epsilon\mathbf{v}_1 + o(\epsilon)$. If we further expand also the tilt angle ϕ, long but straightforward calculations provide

$$K\Delta\phi_1 - \gamma_1 v_0\,\phi_{1,x} - \chi_a H^2\phi_1\cos 2\phi_0 = \gamma_1 v_1\,\phi_{0,x} - \gamma_1\omega_1 + \gamma_2\,\mathbf{n}_{\perp 0}\cdot\mathbf{D}\mathbf{n}_0.$$

4 Variational dissipation principle

In this section we make use of the Dissipation Principle, postulated by Leonov in 2005. In [46], he proved that the Euler equations for the minimisers of an extended dissipative functional coincide with the Stokes equations for the Leslie–Ericksen dynamic theory of nematic liquid crystals. The dissipation functional to be minimised differs from the classical dissipation functional of nematic liquid crystals by a term proportional to the divergence of the velocity field, and the validity of the proof rests upon the hypothesis that the flows occur at low Reynolds number. This latter hypothesis was already present in the derivation of the no-backflow results in [32]: it is crucial for the very existence of a stationarily moving pattern. A corollary of the above principle allows us to explicitly construct approximate solutions for the velocity field.

Variational principle. Consider a pattern $\{\mathbf{n}, \mathbf{u}, p\}$, moving stationarily along the x-direction in the sense of equation (2.6). Assume further that it exists $\mathbf{u}_0$ such that $\mathbf{u}(\mathbf{x}) \to \mathbf{u}_0$ as $|x| \to +\infty$. Then, the actual velocity field $\mathbf{u}$ minimises $\mathscr{D}$ (the dissipation functional) at fixed director field. In particular, $\delta\mathscr{D} = 0$ for any infinitesimal perturbation $\delta\mathbf{u}$ of the backflow field, which preserves the boundary conditions at infinity, and satisfies $\operatorname{div}\delta\mathbf{u} = 0$.

The dissipation function of a nematic liquid crystal is given by

$$\mathscr{D} = T\dot{S} = \int_{\mathbf{R}^2}(\mathbf{D}\cdot\mathbf{T}^{(i)} + \mathbf{h}\cdot\mathbf{N})da,$$

where $\mathbf{D}$ is the rate of strain tensor, and $\mathbf{T}^{(i)}$, $\mathbf{N}$ and $\mathbf{h}$ are defined in equations (2.2)–(2.3). If we now make use of the perturbative expansion (3.1)–(3.2), we obtain $\mathscr{D} = \mathscr{D}_0 + \epsilon\mathscr{D}_1 + o(\epsilon)$,

https://doi.org/10.1017/S0956792510000343 Published online by Cambridge University Press

with

$$\mathscr{D}_0 = \gamma_1 \int_{\mathbf{R}^2} \mathbf{N}_0 \cdot \mathbf{N}_0 \, da = \gamma_1 \int_{\mathbf{R}^2} (\boldsymbol{\nabla}\phi_0 \cdot \mathbf{v}_0)^2 \, da, \quad \text{and}$$

$$\mathscr{D}_1 = \int_{\mathbf{R}^2} (\tilde{\alpha}_4 \, |\mathbf{D}_1|^2 + 2\gamma_2 \, \mathbf{D}_1\mathbf{N}_0 \cdot \mathbf{n}_0 + 2\gamma_1 \, \mathbf{N}_0 \cdot \mathbf{N}_1) da,$$

where $\mathbf{D}_1 = \operatorname{sym} \boldsymbol{\nabla}\mathbf{u}_1$, and

$$\mathbf{N}_1 = \dot{\mathbf{n}}_1 - \boldsymbol{\omega}_1 \wedge \mathbf{n}_0 = -(\boldsymbol{\nabla}\mathbf{n}_1)\mathbf{v}_0 - (\boldsymbol{\nabla}\mathbf{n}_0)\mathbf{v}_1 - \boldsymbol{\omega}_1 \wedge \mathbf{n}_0.$$

Thus,

$$\begin{aligned}
\mathscr{D}_1 &= \int_{\mathbf{R}^2} (\tilde{\alpha}_4 \, |\mathbf{D}_1|^2 - 2\gamma_2 \, \mathbf{D}_1(\boldsymbol{\nabla}\mathbf{n}_0)\mathbf{v}_0 \cdot \mathbf{n}_0 + 2\gamma_1 \, (\boldsymbol{\nabla}\mathbf{n}_0)\mathbf{v}_0 \cdot \boldsymbol{\omega}_1 \wedge \mathbf{n}_0 \\
&\quad + 2\gamma_1 \, (\boldsymbol{\nabla}\mathbf{n}_0)\mathbf{v}_0 \cdot (\boldsymbol{\nabla}\mathbf{n}_1)\mathbf{v}_0 + 2\gamma_1 \, (\boldsymbol{\nabla}\mathbf{n}_0)\mathbf{v}_0 \cdot (\boldsymbol{\nabla}\mathbf{n}_0)\mathbf{v}_1) da, \\
&= \int_{\mathbf{R}^2} (\tilde{\alpha}_4 \, |\mathbf{D}_1|^2 - 2\gamma_2 v_0 \phi_{0,x} \, \mathbf{D}_1\mathbf{n}_{0\perp} \cdot \mathbf{n}_0 + 2\gamma_1 v_0 \phi_{0,x} \omega_1) da \\
&\quad + \text{terms depending on field and velocity corrections.}
\end{aligned} \tag{4.1}$$

The presence, in equation (4.1), of terms linear in the velocity field is already sufficient to show that the backflow may be able to reduce the dissipation.

5 Velocity field around a disclination

In this section we will apply the methods introduced above to a particular example: the backflow field around a moving disclination. The problem, in the absence of backflow, has been already studied in [32], in which the present authors have obtained a solution of the stationary equation (3.3) which represents a $\pm\frac{1}{2}$ moving disclination, placed at the origin of the co-moving reference frame. In order to cover both disclination signs, we introduce a parameter $\eta = \pm\frac{1}{2}$. Then the director field around a disclination with tolopogical charge η is explicitly given by

$$\begin{aligned}
&\phi_0(x, y) = \frac{\eta\pi}{2} \, \mathrm{e}^{-\frac{y}{\xi}} - \eta \int_0^{+\infty} \operatorname{Im} \mathrm{e}^{\mathrm{i}qx - k_q y} \, \frac{dq}{q} \quad \text{if } y \geqslant 0, \\
&\phi_0(x, y) = -\phi_0(x, -y) \quad \text{otherwise,}
\end{aligned} \tag{5.1}$$

where $\xi := \sqrt{K/(\chi_a H^2)}$ and k_q denote the positive real-part square root of the equation $k_q^2 = q^2 + \mathrm{i}q\gamma + \xi^{-2}$, with $\gamma = \gamma_1 v_0/(2K)$. The zero-th order approximation to the speed of the moving disclination is determined through the self-consistency equation

$$\int_0^{\xi q_{\max}} \frac{\sqrt{k^2 + \mathrm{i}k\lambda + 1} - \sqrt{k^2 - \mathrm{i}k\lambda + 1}}{k} \, dk = \mathrm{i}\pi,$$

where $\lambda = \gamma\xi$, and a high-q cutoff is needed in order to avoid the logarithmic divergence that the disclination induces both in the free energy and the dissipation.

https://doi.org/10.1017/S0956792510000343 Published online by Cambridge University Press

5.0.2 *Planar incompressible velocity fields*

We begin by expanding the velocity field $\mathbf{u}_1$ in Fourier series with respect to the polar angle θ

$$\mathbf{u}_1(r,\theta) = \mathbf{f}_0(r) + \sum_{n=1}^{\infty} (\mathbf{f}_n(r)\cos n\theta + \mathbf{g}_n(r)\sin n\theta).$$

The symmetry of the problem requires that the component u_{1x} has to be even, and the u_{1y} has to be odd, with respect to the y coordinate. Thus,

$$\mathbf{u}_1(r,\theta) = \left(f_0(r) + \sum_{n=1}^{\infty} f_n(r)\cos n\theta\right)\mathbf{e}_x + \left(\sum_{n=1}^{\infty} g_n(r)\sin n\theta\right)\mathbf{e}_y. \tag{5.2}$$

In the following we will use expression (5.2) to compute $\mathscr{D}_1$, the first-order contribution to the dissipation functional. The rate of strain tensor is given by

$$\begin{aligned}
\mathbf{D}_1 = \operatorname{sym}\nabla\mathbf{u}_1 \quad = \quad & \frac{1}{2}\left(f_0'(r) + \sum_{n=1}^{\infty} f_n'(r)\cos n\theta\right)(\mathbf{e}_x\otimes\mathbf{e}_r + \mathbf{e}_r\otimes\mathbf{e}_x) \\
& - \frac{1}{2}\left(\sum_{n=1}^{\infty}\frac{nf_n(r)}{r}\sin n\theta\right)(\mathbf{e}_x\otimes\mathbf{e}_\theta + \mathbf{e}_\theta\otimes\mathbf{e}_x) \\
& + \frac{1}{2}\left(\sum_{n=1}^{\infty} g_n'(r)\sin n\theta\right)(\mathbf{e}_y\otimes\mathbf{e}_r + \mathbf{e}_r\otimes\mathbf{e}_y) \\
& + \frac{1}{2}\left(\sum_{n=1}^{\infty}\frac{ng_n(r)}{r}\cos n\theta\right)(\mathbf{e}_y\otimes\mathbf{e}_\theta + \mathbf{e}_\theta\otimes\mathbf{e}_y).
\end{aligned}$$

The incompressibility condition may be directly enforced in terms of the f_n and g_n components. A direct computation and the repeated use of the Werner formulae yields

$$\begin{aligned}
\operatorname{div}\mathbf{u}_1 = \operatorname{tr}\mathbf{D}_1 = f_0'\cos\theta + \frac{1}{2}\sum_{n=0}^{\infty}\left(s_{n+1}' + \frac{(n+1)s_{n+1}}{r}\right)\cos n\theta \\
+ \frac{1}{2}\sum_{n=2}^{\infty}\left(d_{n-1}' - \frac{(n-1)d_{n-1}}{r}\right)\cos n\theta,
\end{aligned}$$

where we have introduced the notations

$$s_n(r) := f_n(r) + g_n(r), \qquad d_n(r) := f_n(r) - g_n(r) \qquad \forall n \geqslant 1. \tag{5.3}$$

Therefore, the requirement $\operatorname{div}\mathbf{u}_1 = 0$ is equivalent to the following set of conditions

$$\begin{aligned}
& s_1' + \frac{s_1}{r} = 0, \\
& s_2' + \frac{2s_2}{r} = -2f_0', \\
& s_n' + \frac{ns_n}{r} = -d_{n-2}' + \frac{(n-2)d_{n-2}}{r} \qquad (\forall n \geqslant 3).
\end{aligned} \tag{5.4}$$

https://doi.org/10.1017/S0956792510000343 Published online by Cambridge University Press

Equation $(5.4)_1$ may be directly integrated as

$$s_1(r) = \frac{2E_1}{r}, \quad E_1 \in \mathbb{R}.$$

The remaining equations allow to show that once the differences d_n are determined, the sums s_n follow from the incompressibility constraint.

In order to compute the dissipation functional, we also determine the vorticity vector $\boldsymbol{\omega}_1 = \omega_1 \, \mathbf{e}_z$:

$$\begin{aligned} \omega_1 &= \frac{1}{4}\left(s_2' + \frac{2s_2}{r} - 2f_0'\right)\sin\theta \\ &\quad + \frac{1}{4}\sum_{n=2}^{\infty}\left(s_{n+1}' + \frac{(n+1)s_{n+1}}{r} - d_{n-1}' + \frac{(n-1)d_{n-1}}{r}\right)\sin n\theta \\ &= -f_0'\sin\theta - \frac{1}{2}\sum_{n=1}^{\infty}\left(d_n' - \frac{nd_n}{r}\right)\sin(n+1)\theta, \end{aligned}$$

where in the last equality we have made use of the incompressibility conditions (5.4). We can therefore write

$$\omega_1(r,\theta) = \sum_{n=0}^{\infty}\omega_{1,n}(r)\sin(n+1)\theta$$

with

$$\omega_{1,0}(r) = -f_0'(r), \quad \text{and} \quad \omega_{1,n}(r) = -\frac{1}{2}\left(d_n' - \frac{nd_n}{r}\right) \quad \text{for} \quad n \geqslant 1.$$

5.0.3 *Ansatz*

We now introduce a simple ansatz that provides insight into the structure and the symmetry of the velocity pattern around a moving disclination. Since the aim of the present paper is to introduce a new perturbative computational method, we will keep the ansatz as simple as possible. In fact, we will truncate our approximations at the first non-trivial order, though we stress that the method can be easily generalised to produce a more refined ansatz that eventually allows to approximate the correct solution within any prescribed precision.

We assume that the Fourier components of the vorticity vector $\omega_{1,n}$ are (as functions of r) piecewise polynomials of order N. The number of different polynomials we glue, and the order of each polynomial determine the complexity (and the precision) of the particular ansatz. The simplest non-trivial choice consists in assuming that each $\omega_{1,n}$ is a piecewise constant function that assumes a constant value within a disk of radius R (that will be called the *vorticity disk*), and vanishes when $r > R$

$$\omega_{1,n}(r) = \begin{cases} D_n & \text{if } r < R \\ 0 & \text{if } r > R \end{cases}, \tag{5.5}$$

with $D_n \in \mathbb{R}$ for all $n \geqslant 0$. The real parameters to be determined variationally in the present ansatz are the radius R and the values D_n that each component assumes within the

https://doi.org/10.1017/S0956792510000343 Published online by Cambridge University Press

vorticity disk. We remark that the outcoming vorticity field is a piecewise regular function, with a jump discontinuity at the border $r = R$. Once we integrate, the resulting velocity field is continuous everywhere. Higher ansatz orders that allow for regular vorticity fields will be presented elsewhere [51].

Once the choice (5.5) is set, all the components d_n can be determined by solving the ordinary differential equations,

$$f_0' \equiv -\omega_{1,0}, \qquad d_n' - \frac{n\, d_n}{r} \equiv -2\omega_{1,n} \quad \forall n \geqslant 1,$$

subject to the conditions ensuring that f_0 and all the d_ns are continuous everywhere, and vanish at infinity. If we use the resulting d_ns to deduce the s_ns by solving (5.4), and eventually invert the definitions (5.3), we obtain

$$\begin{array}{ll}
r \leqslant R & r > R, \\
f_0(r) = D_0(R - r) & f_0(r) = 0, \\
f_1(r) = D_1\, r\, \log \dfrac{R}{r} & f_1(r) = 0, \\
g_1(r) = -D_1\, r\, \log \dfrac{R}{r} & g_1(r) = 0, \\
f_2(r) = \dfrac{D_0 r}{3} + \dfrac{D_2 r(R-r)}{R} & f_2(r) = \dfrac{D_0 R^3}{3r^2}, \\
g_2(r) = \dfrac{D_0 r}{3} - \dfrac{D_2 r(R-r)}{R} & g_2(r) = \dfrac{D_0 R^3}{3r^2}, \\
\ldots \quad \ldots & \ldots \quad \ldots \\
f_n(r) = \dfrac{D_{n-2} r}{n+1} + \dfrac{D_n r(R^{n-1} - r^{n-1})}{(n-1)R^{n-1}} & f_n(r) = \dfrac{D_{n-2} R^{n+1}}{(n+1)r^n}, \\
g_n(r) = \dfrac{D_{n-2} r}{n+1} - \dfrac{D_n r(R^{n-1} - r^{n-1})}{(n-1)R^{n-1}} & g_n(r) = \dfrac{D_{n-2} R^{n+1}}{(n+1)r^n}. \\
\ldots \quad \ldots & \ldots \quad \ldots
\end{array} \tag{5.6}$$

It is interesting to remark that by virtue of (5.6) the velocity field *at* the disclination, i.e. in the origin, depends only on the value of D_0

$$\mathbf{u}_1(\mathbf{0}) = D_0 R \mathbf{e}_x. \tag{5.7}$$

5.0.4 *Reducing the dissipation*

In this section we explicitly compute the terms in the dissipation functional that depend on the velocity field. They are

$$\mathscr{D}_1^{(\mathbf{u})} = \int_{\mathbf{R}^2} (\tilde{\alpha}_4 |\mathbf{D}_1|^2 - 2\gamma_2\, \mathbf{D}_1(\nabla \mathbf{n}_0)\mathbf{v}_0 \cdot \mathbf{n}_0 + 2\gamma_1\, (\nabla \mathbf{n}_0)\mathbf{v}_0 \cdot \boldsymbol{\omega}_1 \wedge \mathbf{n}_0) da. \tag{5.8}$$

The quadratic term, proportional to $|\mathbf{D}_1|^2$, is positively defined. The presence of this classical viscosity term keeps the velocity field bounded. Once we make use of (5.6), it

https://doi.org/10.1017/S0956792510000343 Published online by Cambridge University Press

turns out that it can be easily computed

$$\tilde{\alpha}_4 \int_{\mathbf{R}^2} \mathbf{D}_1 \cdot \mathbf{D}_1 \, \mathrm{d}a = \pi R^2 \tilde{\alpha}_4 \sum_{n=0}^{+\infty} D_n^2. \tag{5.9}$$

The result (5.9) is not surprising from the physical point of view, because it is clear that the overall dissipation increases if we either increase the size of the vorticity disk where $\boldsymbol{\omega}_1$ is confined, or increase the intensities of the vorticity Fourier components.

The linear γ_1 and γ_2 terms in (5.8) are crucial. They couple the velocity and the director fields, and allow a reduction of the overall dissipation simply because of their linear character. Were they absent, the quadratic term in the dissipation functional would keep the optimal velocity field null. Moreover, since these terms are linear in $\mathbf{u}$, each Fourier component can be treated in it independently. In particular, only a few Fourier components will have the correct symmetry that allows the integrals in (5.8) to be different from zero. Consequently, only a few Fourier components will have a non-zero optimal value for the variational parameters D_n.

An exact computation of the γ_1 and γ_2 integrals in (5.8) cannot produce interpretable results easily because they involve integrals of the tilt field ϕ, which in turn is known only through its Fourier transform. Thus, again, we resort to a physical approximation, and postpone the complete results to a forthcoming paper [51]. The resulting predictions will be used to check the validity of the present assumptions.

First of all, we assume that most of the dissipation reduction occurs close to the (co-moving) origin, where the disclination stands. This assumption is due to the fact that the dissipation is indeed concentrated at the disclination, and thus it is to be expected that the dissipation reduction is greater where the dissipation is high. In practice, we will replace the integrals over the whole plane $\mathscr{B}$ with integrals over the vorticity disk $\mathscr{B}_R = \{r \leqslant R\}$. We stress that we perform this approximation only in the linear terms, which represent the gain, while we take into account the whole plane when we compute the quadratic dissipation term. Moreover, we remark that this approximation does not contribute to the γ_1-integral, since in the latter the integral is proportional to the vorticity, and $\boldsymbol{\omega}_1$ vanishes outside $\mathscr{B}_R$. Then we assume that R is sufficiently small so that within it the tilt field can be replaced by its asymptotic expression, $\phi_0 \approx \eta\theta$, where we remind that $\eta = \pm\frac{1}{2}$ is the topological charge of the defect that we are considering.

Under the above assumptions, the γ_1-linear term in (5.8) yields

$$\int_{\mathscr{B}_R} 2\gamma_1 \, (\boldsymbol{\nabla}\mathbf{n}_0)\mathbf{v}_0 \cdot \boldsymbol{\omega}_1 \wedge \mathbf{n}_0 \, da = 2v_0\gamma_1 \int_{\mathscr{B}_R} \phi_{0,x}\omega_1 \, da = -2\eta\pi\gamma_1 v_0 D_0 R. \tag{5.10}$$

The result (5.10) deserves a remark. It shows that only the principal component $\omega_{1,0}$ of the vorticity possesses the correct symmetry to determine a reduction in the overall dissipation. All other components do not contribute to the linear dissipation gain – while they obviously still cause a dissipation increase because of the positive quadratic term. The gain can be obtained, whatever is the sign of the topological charge of the disclination, since defects with opposite charges will simply induce opposite velocity fields. It is to be noticed that changing the sign of D_0 induces an important effect. In view of (5.7), and since the disclination moves with a velocity $\mathbf{v}_0 = v_0\mathbf{e}_x$, disclinations which D_0 with the

https://doi.org/10.1017/S0956792510000343 Published online by Cambridge University Press

same sign as v_0 encounter a velocity field parallel to their motion. In some figurative sense they sail before the wind. On the contrary, disclinations which induce D_0 opposite in sign as compared to v_0 will sail against the backflow motion. We will return on this point, but we remark that this is the effect for understanding the speed difference between opposite-charged defects.

The linear γ_2-term provides

$$-2\gamma_2 \int_{\mathscr{B}_R} \mathbf{D}_1(\boldsymbol{\nabla}\mathbf{n}_0)\mathbf{v}_0 \cdot \mathbf{n}_0 \, \mathrm{d}a = -\frac{\pi\gamma_2 v_0 R}{2}\big(D_1 + \big(\eta - \tfrac{1}{2}\big)D_3\big). \tag{5.11}$$

In this case it is interesting to be noticed that the value of the topological charge $\eta = \pm\frac{1}{2}$ enters the result in a non-trivial way. The Fourier component represented by D_1 induces a dissipation reduction independent of η. Thus, the D_1 component will have the same sign for both positive- and negative-charged disclination. Consequently, it will not be true that the velocity field induced by one disclination is just the opposite of the velocity field induced by its opposite-charged counterpart. Moreover, the dissipation gain induced by the third Fourier component D_3 is proportional to the factor $(\eta - \frac{1}{2})$. As a consequence, a positive-charged disclination will not find any convenience in switching on this component. On the contrary, the $\eta = -\frac{1}{2}$ disclination will find its way to save dissipation with a suitable velocity field endowed with this component. This result confirms and provides an explicit example of our physical intuition that the $\eta = -\frac{1}{2}$ disclinations possess a three-fold symmetry about the disclination axis.

In summary, the optimal values for the velocity coefficients can be found by adding the contributions (5.9), (5.10) and (5.11), and minimising with respect to the D_ns:

$$D_{0,\mathrm{opt}} = \frac{\eta\gamma_1 v_0}{R\tilde{\alpha}_4}, \qquad D_{1,\mathrm{opt}} = \frac{\gamma_2 v_0}{4R\tilde{\alpha}_4}, \qquad D_{3,\mathrm{opt}} = \frac{\gamma_2 v_0(\eta - \frac{1}{2})}{4R\tilde{\alpha}_4}, \tag{5.12}$$

while $D_{n,\mathrm{opt}} = 0$ for all other values of n.

Within our approximation, the components D_n always enter the dissipation gain $\mathscr{D}_1$ through the combination RD_n. Thus, it was to be expected that their optimal values were always proportional to R^{-1}. Moreover, once we replace the optimal values (5.12) in $\mathscr{D}_1$, we obtain a dissipation gain that does not depend on the particular value of the radius R of the vorticity disk

$$\mathscr{D}_{1,\mathrm{opt}} = -\frac{\pi v_0^2}{16\tilde{\alpha}_4}\big(4\gamma_1^2 + \gamma_2^2\big(1 + \big(\eta - \tfrac{1}{2}\big)^2\big)\big). \tag{5.13}$$

5.0.5 *Backflow vortices*

The approximations introduced above have yielded some non-trivial insight into the structure of the velocity field. The positive-charged disclinations move *downstream*, while the negative-charged disclinations are forced to go *upstream*, but we have not yet obtained any estimate for the optimal radius of the vorticity disk. One assumption that has played a key role in deriving the above results is that within the vorticity disk the director field can be approximated as $\phi_0(r,\theta) \approx \eta\theta$, i.e. we may replace the exact director field with its asymptotic expression valid close to the defect. In this section we will relax this

https://doi.org/10.1017/S0956792510000343 Published online by Cambridge University Press

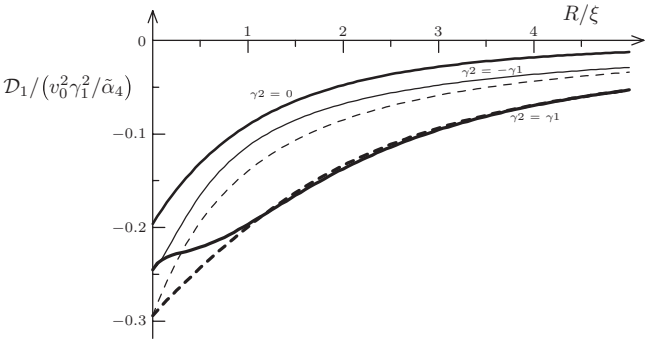

FIGURE 1. Dissipation gain induced by the velocity flow for a positive- (continuous plots) and negative-charged (dashed plots) disclinations as a function of the radius of the vorticity disk. Different plots correspond to different values of the dimensionless ratio γ_2/γ_1. When $\gamma_2 = 0$, the continuous and dashed plots coincide.

assumption. As a result, we will be able to determine the optimal value of the radius of the vorticity disk.

Once the expression (5.1) replaces its asymptotic approximation, the dependence on the radius R of the vorticity disk of the dissipation gain can not be obtained analytically. We have computed numerically for several values of $R \leqslant 5\xi$ (with step size 0.01ξ, where ξ is the magnetic coherence length introduced in (5.1)) and for all Fourier components controlled by D_n (up to $n_{\max} = 50$), the integrals appearing on the left-hand sides of equations (5.10) and (5.11). From these, we have derived their optimal values $D_{n,\mathrm{opt}}(R)$. Finally, we have added all the contributions to obtain $\mathscr{D}_{1,\mathrm{opt}}(R)$, the counterpart of equation (5.13). Again, using the exact director field results in a non-constant $\mathscr{D}_{1,\mathrm{opt}}(R)$. Figure 1 illustrates the result of our calculations. Once we factor out the coefficient $v_0^2\gamma_1^2/\tilde{\alpha}_4$, the optimal dissipation gain depends on the dimensionless ratios R/ξ and γ_2/γ_1.

The dissipation gain is greater when $\mathscr{D}_1$ is most negative. Thus, the main feature of all graphs is that the dissipation gain is maximum when R is as small as possible and, in all cases, the optimal situation corresponds to the $R \to 0$ limit. This means that the most effective way to reduce the dissipation is to concentrate the vorticity in a disk as small as possible around the disclination. Incidentally, if the radius is small, the results (5.10)–(5.13) come up again, because within a disk of infinitesimal radius the approximation $\phi_0 \approx \eta\theta$ regains validity. In particular, equation (5.12) show that the non-zero $D_{n,\mathrm{opt}}$s diverge if $R \to 0$, while the products $RD_{n,\mathrm{opt}}$ remain finite. In this limit, the vorticity disk thus turns into the combination of two or three *vortices* (depending on the sign of the topological charge of the disclination), each endowed with a different Fourier symmetry. The analytical estimate (5.13) corresponds to the $R \to 0$ limit of the curves in Figure 1, which explains the fact that the plots with $\gamma_2 = \pm\gamma_1$, but with the same topological charge, converge to the same value in the small-R limit. On the contrary, it is interesting to note that when R increases, plots with the same value of the ratio γ_2/γ_1, but with opposite topological charge, tend to coalesce.

Figure 2 illustrates the qualitative features of the velocity field induced by the disclination motion. It evidences that the velocity field of the $-\frac{1}{2}$ defect reflects the three-fold

https://doi.org/10.1017/S0956792510000343 Published online by Cambridge University Press

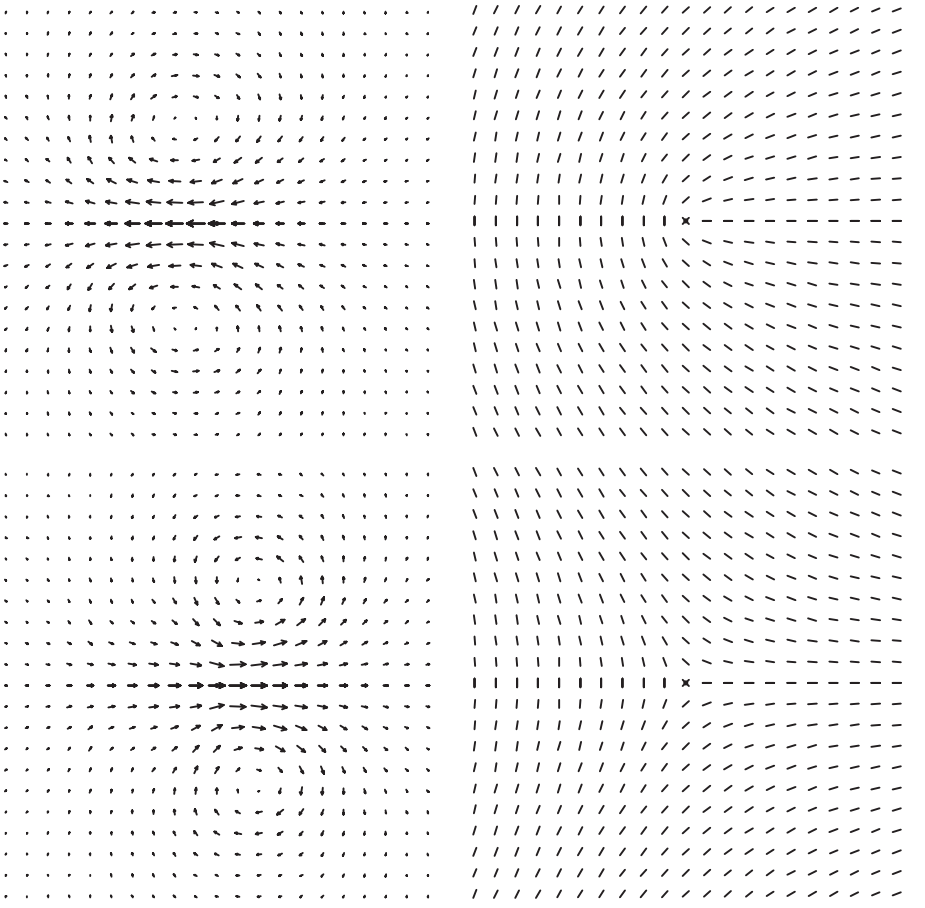

FIGURE 2. Velocity fields (left) for a $+\frac{1}{2}$ defect (upper) and a $-\frac{1}{2}$ defect (lower). The displayed fields have been obtained with a small though finite value of the vorticity disk ($R = .1\xi$). Both defects move towards the left side. The right panels show the director field close to a $\pm\frac{1}{2}$ defect.

symmetry of the director field. The points where the velocity is greater sit in front of the $+\frac{1}{2}$ defect, but behind the $-\frac{1}{2}$ defect (with respect to the direction of motion). More precisely, let us consider the apparent *centres of rotation*, defined as the points where the velocity field vanishes. Let us then draw the lines from such centres to the defect itself, and consider the negative x-axis (the π-wall) as well. In the $R \to 0$ limit, these three lines form three equal angles of $\frac{2}{3}\pi$. (Note that in Figure 2, the value of R is small but finite, and therefore the symmetry is approximate.)

6 Conclusions

We have introduced a perturbative scheme aimed at taking into account the backflow effects in the dynamics of nematic liquid crystals. The key idea in the expansion is to notice that the no-backflow approximation is equivalent to assuming that the ratio between the

https://doi.org/10.1017/S0956792510000343 Published online by Cambridge University Press

Newtonian viscosity α_4 and all other nematic viscosities is very large. As a consequence, it turns out that the onset of backflow effects is principally governed by two of the dissipative terms in the stress tensor (the ones proportional to α_2 and α_3). The resulting equations of motion (see equations (3.4) and (3.5)) appear to be simplified as compared to the original balance equations, though they still do not admit an analytical solution.

In Section 4, we have adapted to our problem, the variational dissipation principle proved by Leonov [46]. In view of this theorem, the actual velocity field $\mathbf{u}$ is a minimiser of the dissipation functional at fixed director field. This property allows us to determine analytical estimates of the actual solution.

In Section 5 we applied the above results to a practical example: the velocity field induced by a moving disclination. By means of a suitable variational ansatz, we have restricted to velocity fields whose vorticity is bounded within a *vorticity disk*, whose radius we have estimated. Though we have kept the ansatz as simple as possible, non-trivial results already emerge. Two of these deserve particular mention. First, the velocity field tends to form vortices, endowed with non-trivial Fourier structure. The number and character of the vortices depend on the topological charge of the disclinations. Second, the sign of the velocity field *at* the disclination depends on the sign of the charge itself. More precisely, a moving disclination with positive charge encounters a drift coherent with the direction of the disclination velocity, while a negative-charged disclination is forced to overcome an opposite drift.

Since $\mathbf{u}_1(\mathbf{0}) = (\eta\gamma_1 v_0/\tilde{\alpha}_4)\,\mathbf{e}_x$, we may expect that the difference in velocity speeds (noticed both in numerical simulation and in experimental measurements) between approaching $\pm\frac{1}{2}$ defects can be estimated as $\Delta v_1 \approx (\gamma_1 v_0)/\tilde{\alpha}_4$. This result obviously needs to be confirmed when more refined ansatzs are considered, but it explains the origin of the numerical and experimental observations.

Our study evidences that the dissipation reduction arising from the backflow effects emerges from the terms highlighted in equation (5.8). Even the most simple study of their optimisation underlines the key role played by the topological charge of the moving defect, and the symmetry of the nematic field that surrounds the singularity. The origin of the predicted and measured different defect speeds is to be found in the fact that defects turn out to move either downhill or uphill (with respect to the backflow motion), depending on the sign of their topological charge.

Much work remains, however, to be done to fully understand the defect motion. A more complete velocity ansatz would certainly evidence that the vortices we have predicted are combined with a regular pattern, whose characteristic length must clearly depend on the magnetic coherence length ξ. Moreover, it still remains to be understood how the backflow perturbation of the defect speed (the parameter v_1 in our notation) depends on two effects: the dissipation reduction induced by the backflow, and the difference $\mathbf{v}_0 - \mathbf{u}(\mathbf{0})$. Finally, a three-dimensional implementation of the program we have carried out would result in a better understanding of the motion of point defects in a velocity field.

Acknowledgement

One of the Authors (TJS) wishes to thank the Italian *Istituto Nazionale di Alta Matematica* for having supported his visit to Milan.

References

[1] Friedel, G. (1922) (Extracts from) Les états mésomorphes de la matière (The mesomorphic states of matter). *Ann. Phys. – Paris* **18**, 273–474.

[2] Mermin, N. D. (1979) The topological theory of defects in ordered media. *Rev. Mod. Phys.* **51**, 591–648.

[3] Kléman, M. (1989) Defects in liquid crystals. *Rep. Prog. Phys.* **52**, 555–654.

[4] Kléman, M. & Friedel, J. (2008) Disclinations, dislocations, and continuous defects: A reappraisal. *Rev. Mod. Phys.* **80**, 61–115.

[5] Biscari, P. & Guidone Peroli, G. (1997) A hierarchy of defects in biaxial nematics. *Commun. Math. Phys.* **186**, 381–392.

[6] Oseen, C. W. (1933) The theory of liquid crystals. *Trans. Faraday Soc.* **29**, 883–900.

[7] Frank, F. C. (1958) On the theory of liquid crystals. *Disc. Faraday Soc.* **25**, 19–28.

[8] Ericksen, J. L. (1961) Hydrostatic theory of liquid crystals. *Arch. Ration. Mech. Anal.* **9**, 371–378.

[9] Ericksen, J. L. (1961) Anisotropic fluids. *Arch. Ration. Mech. Anal.* **9**, 231–237.

[10] Ericksen, J. L. (1962) Nilpotent energies in liquid crystal theory. *Arch. Ration. Mech. Anal.* **10**, 189–196.

[11] Leslie, F. M. (1968) Some constitutive equations for liquid crystals. *Arch. Rat. Mech. Anal.* **28**, 265–283.

[12] de Gennes, P. G. (1971) Short-range order effects in the isotropic phase of nematics and cholesterics. *Mol. Cryst. Liq. Cryst.* **12**, 193–214.

[13] Olmsted, P. D. & Goldbartr, P. (1990) Theory of the non-equilibrium phase transition for nematic liquid crystals under shear flow. *Phys. Rev.* A **41**, 4578–4581.

[14] Olmsted, P. D. & Goldbart, P. (1992) Isotropic-nematic transition in shear flow: State selection, coexistence, phase transitions, and critical behaviour. *Phys. Rev.* A **46**, 4578–4993.

[15] Beris, A. N. & Edwards, B. J. (1994) *Thermodynamics of Flowing Systems with Internal Microstructure*, Oxford University Press, Oxford, UK.

[16] Schopohl, N. & Sluckin, T. J. (1987) Defect core structure in nematic liquid crystals. *Phys. Rev. Lett.* **59**, 2582–2584.

[17] Volterra, V. (1905) Sull'equilibrio dei corpi elastici più volte connessi. *Rend. R. Acc. Lincei* **14**, 193–202.

[18] Love, A. E. H. (1927) *A Treatise on the Mathematical Theory of Elasticity*, 4th ed., Cambridge University Press, Cambridge, UK.

[19] Burgers, J. M. (1939) Some considerations of the field of stress connected with dislocations in a regular crystal lattice. *K. Ned. Akad. Wet.* **42**, 293–325 (Part I), 378–399 (Part II).

[20] Ryskin, G. & Kremenetsky, M. (1991) Drag force on a line defect moving through an otherwise undisturbed field: Disclination line in a nematic liquid crystal. *Phys. Rev. Lett.* **67**, 1574–1577.

[21] Denniston, C. (1996) Disclination dynamics in nematic liquid crystals. *Phys. Rev.* B **54**, 6272–6275.

[22] Kats, E. I., Lebedev, V. V. & Malinin, S. V. (2002) Disclination motion in liquid crystalline films. *JETP* **95**, 714–727.

[23] Clark, M. G. & Leslie, F. M. (1978) A calculation of orientational relaxation in nematic liquid crystals. *Proc. R. Soc. Lond.* A **361**, 463–485.

[24] Pargellis, A., Turok, N. & Yurke, B. (1991) Monopole–antimonopole annihilation in a nematic liquid crystal. *Phys. Rev. Lett.* **67**, 1570–1573.

[25] Yakutovich, M. V., Newton, C. J. P. & Cleaver, D. J. (2009) Mesh-free simulation of complex LCD geometries. *Mol. Cryst. Liq. Cryst.* **502**, 245–257.

[26] Pismen, L. M. & Rubinstein, B. Y. (1992) Motion of interacting point defects in nematics. *Phys. Rev. Lett.* **69**, 96–99.

[27] Guidone Peroli, G. & Virga, E. G. (1996) Annihilation of point defects in nematic liquid crystals. *Phys. Rev.* E **54**, 5235–5241.

[28] Guidone Peroli, G. & Virga, E. G. (1998) Dynamics of point defects in nematic liquid crystals. *Physica* D **111**, 356–372.
[29] Biscari, P., Guidone Peroli, G. & Virga, E. G. (1999) A statistical study for evolving arrays of nematic point defects. *Liq. Cryst.* **26**, 1825–1832.
[30] Hindmarsh, M. (1995) Where are the hedgehogs in quenched nematics? *Phys. Rev. Lett.* **75**, 2502–2505.
[31] Richardson, G. (2000) Line disclination dynamics in uniaxial nematic liquid crystals. *Q. Jl. Mech. Appl. Math.* **53**, 49–71.
[32] Biscari, P. & Sluckin, T. J. (2005) Field-induced motion of nematic disclinations. *SIAM J. Appl. Math.* **65**, 2141–2157.
[33] Denniston, C., Orlandini, E. & Yeomans, J. M. (2000) Simulations of liquid crystal hydrodynamics in the isotropic and nematic phases. *Europhys. Lett.* **52**, 481–487.
[34] Denniston, C., Orlandini, E. & Yeomans, J. M. (2001) Lattice Boltzmann simulations of liquid crystal hydrodynamics. *Phys. Rev.* E **63**, 056702.
[35] Tóth, G., Denniston, C. & Yeomans, J. M. (2002) Hydrodynamics of topological defects in nematic liquid crystals. *Phys. Rev. Lett.* **88**, 105504.
[36] Svenšek, D. & Žumer, S. (2002) Hydrodynamics of pair-annihilating disclination lines in nematic liquid crystals. *Phys. Rev.* E **66**, 021712.
[37] Blanc, C., Svensek, D., Zumer, S. & Nobili, M. (2005) Dynamics of nematic liquid crystal disclinations: The role of the backflow. *Phys. Rev. Lett.* **95**, 097802.
[38] Grecov, D. & Rey, A. D. (2004) Impact of texture on stress growth in thermotropic liquid crystalline polymers subjected to step-shear. *Rheol. Acta* **44**, 135–149.
[39] Liu, C., Shen, J. & Yang, X.-F. (2007) Dynamics of defect motion in nematic liquid crystal flow: Modeling and numerical simulation. *Commun. Comput. Phys.* **2**, 1184–1198.
[40] Abukhdeir, N. M. & Rey, A. D. (2008) Defect kinetics and dynamics of pattern coarsening in a two-dimensional smectic-A system. *N. J. Phys.* **10**, 063025.
[41] Shoarinejad, S. & Shahzamanian, M. A. (2008) On the numerical study of Frederick transition in nematic liquid crystals. *J. Mol. Liq.* **138**, 14–19.
[42] Kundu, S., Grecov, D., Ogale, A. A. & Rey, A. D. (2009) Shear flow-induced microstructure of a synthetic mesophase pitch. *J. Rheol.* **53**, 85–113.
[43] Viñals, J. (2009) Defect dynamics in mesophases. *J. Phys. Soc. Jpn.* **78**, 041011.
[44] Véron, A. R. & Martins, A. F. (2009) Tensorial form of Leslie–Ericksen equations and applications. *Mol. Cryst. Liq. Cryst.* **508**, 309–336.
[45] Sonnet, A. M. & Virga, E. G. (2009) Flow and reorientation in the dynamics of nematic defects. *Liq. Cryst.* **36**, 1185–1192.
[46] Leonov, A. I. (2005) On the minimum of extended dissipation in viscous nematodynamics. *Rheol. Acta* **44**, 573–576.
[47] de Gennes, P. G. & Prost, J. (1993) *The Physics of Liquid Crystals*, IInd ed., Clarendon Press, Oxford, UK.
[48] Parodi, O. (1970) Stress tensor for a nematic liquid crystal. *J. Physiq.* **31**, 581–584.
[49] Stewart, I. W. (2004) *The Static and Dynamic Continuum Theory of Liquid Crystals*, Ist ed., Taylor & Francis, London.
[50] Majda, A. J. & Bertozzi, A. L. (2002) *Vorticity and incompressible flow*. Cambridge Texts in Applied Mathematics, Ist ed., Vol. 27, Cambridge University Press, Cambridge, UK.
[51] Biscari, P., Sluckin, T. J. & Turzi, S. (2011) (in preparation).